15 Dec 2020

Inter-Cross De-Modulated Refractive Index And Temperature Sensor By An Etched Multi-Core Fiber Of A MZI Structure

Farhan Mumtaz
Missouri University of Science and Technology, mfmawan@mst.edu

Yutang Dai

Muhammad Aqueel Ashraf

Recommended Citation

F. Mumtaz et al., "Inter-Cross De-Modulated Refractive Index And Temperature Sensor By An Etched Multi-Core Fiber Of A MZI Structure," *Journal of Lightwave Technology*, vol. 38, no. 24, pp. 6948 - 6953, article no. 9161269, Institute of Electrical and Electronics Engineers; Optica, Dec 2020.
The definitive version is available at https://doi.org/10.1109/JLT.2020.3014857

Inter-Cross De-Modulated Refractive Index and Temperature Sensor by an Etched Multi-Core Fiber of a MZI Structure

Farhan Mumtaz, Yutang Dai, and Muhammad Aqueel Ashraf

***Abstract*—We present a relative sensitivity of in-fiber inter-cross demodulation of a Mach–Zehnder interferometer (MZI) based on an etched multi-core fiber (eMCF). The sensor can measure the external refractive index (RI) and temperature with a large fringe visibility of 15 dB. It is tuned using a simple technique of slow chemical etching. When the outer cores of MCF will be exposed to the surrounding, a large difference of relative effective RI is observed, which enhances the sensitivity of the sensor. The sensor's wavelength and intensity responses have displayed that it can function with three different inter-cross-demodulation phenomena. A superior RI sensitivity of 178.20 dB/RIU in the range of 1.334 to 1.370, and temperature sensitivity of 66.73 pm/°C in the range of 30 to 80 °C are obtained, with an adequate linear response. Besides, it can readily resolve the issues of cross-sensitivity. Moreover, it has many advantages including easy fabrication, compact size, multiplex, repeatable, stable, and can easily differentiate RI and temperature, which lack others.**

***Index Terms*—Etched Multi-core fiber, inter-cross demodulated refractive index and temperature sensor, mach-zehnder interferometer.**

I. Introduction

NOWADAYS RI and temperature optical sensors [1]–[5] are expanding the research dynamics and becoming a hot-topic interest for industries and research communities. Such sensors are capable of offering easy installation in the numerous practical applications, due to their flexibility and compatibility. With their inherent properties of high sensitivity, compact size, lightweight, electrically passive operation, chemically inert, wide dynamic range, reliable operation, electromagnetic interference immunity, and minimal loss, playing a vital role and making them suitable to be used in various fields of chemical, biological and environmental engineering. A variety of ultra-sensitive RI sensors based on tapered Multi-core fiber (MCF) structures are reported [6]–[8]. MCF has many advantages over single core fibers, it is comprised of multiple cores with in the same cladding. It is supported single mode operation of each core at the same time, such modes are called fundamental super-modes. If the cores are separated far apart, the modal profile overlay may be neglected, and MCF will function as a bundle of single-mode fibers. It is noticeably observed that when the waist of MCF is reduced via tapering or else. In a result, the MCF will face the issues of crosstalk, due to reduction of the pitch among the MCF cores. Therefore, such interferometers will either restrict the measurement range up-to one parameter or offer low cross-sensitivity issues. However, the low cross-sensitivity is a good aspect for dual or multi parameter measurements.

Besides, different principles of RI sensors based on intensity and wavelength demodulation [9]–[14] are reported, including single-multi-single mode (SMS), Fabry–Perot interferometers (FPIs), Michelson interferometers (MI), tilted fiber Bragg gratings (TFBGs), Fabry-Perot (FP), surface plasmon resonance (SPR) and etc. Jing *et al.* [9] has demonstrated an intensity-modulated RI and temperature sensor by a front taper SMS structure, and achieved a relative RI sensitivity of −342.815 dB/RIU in the range of 1.33 to 1.37 and temperature sensitivity of 0.307 dB/°C with a low cross-sensitivity of 0.0002 °C /RIU. Ran *et al.* [10] has presented an FPIs sensor using laser micro-machining, and exhibited a sensitivity of 27 dB/RIU for different RI sensing applications. Xue *et al.* [11] has also demonstrated a MI optical sensor for RI and temperature measurements, and displayed a RI sensitivity as 94.58 dB/RIU and temperature sensitivity as 0.0085 nm/°C. Javier *et al.* [12] has reported a RI and temperature sensor by writing TFBG on MCF, which is used to increase the inter-core crosstalk, and displayed a RI sensitivity of −74.2dB/RIU from 1.31 to 1.39, −250.8 dB/RIU from 1.39 to 1.44 and temperature sensitivity of 9.75 pm/°C from 10 to 40 °C. A FP based sensor [13] is reported with high resolution of RI $\sim 2 \times 10^{-7}$ RIU and temperature $\sim 10^{-3}$ °C by micromachining. González *et al.* [14] explored the SPR sensor, and achieved high refractive index and temperature sensitivity, 2323.4 nm/RIU and −2.850 nm/°C respectively.

Several in-line interferometers based on chemically eMCF are reported [15]–[20]. May-Arrioja *et al.* [15] has experimentally

Manuscript received June 21, 2020; revised July 21, 2020; accepted August 4, 2020. Date of publication August 6, 2020; date of current version December 15, 2020. This work was supported in part by the National Natural Science Foundation of China under Grant 51975442. *(Corresponding author: Yutang Dai.)*

Farhan Mumtaz is with the National Engineering Laboratory for Fiber Optic Sensing Technology, the School of Information and Communication Engineering, Wuhan University of Technology, Wuhan 430070, China, and also with Communications Lab. Department of Electronics, Quaid-i-Azam University, Islamabad 45320, Pakistan (e-mail: mfmawan@yahoo.com).

Yutang Dai is with the National Engineering Laboratory for Fiber Optic Sensing Technology, Wuhan University of Technology, Wuhan 430070, China (e-mail: daiyt6688@whut.edu.cn).

Muhammad Aqueel Ashraf is with the Communications Lab. Department of Electronics, Quaid-i-Azam University, Islamabad 45320, Pakistan (e-mail: aqueel@qau.edu.pk).

Color versions of one or more of the figures in this article are available online at https://ieeexplore.ieee.org.

Digital Object Identifier 10.1109/JLT.2020.3014857

demonstrated an eMCF structure, and displayed a maximum RI sensitivity of 1.25x10^4 nm/RIU. Whereas such structures could able to resolve very small scale RI tracing, i.e., 10^{-4}–10^{-5} with standard laboratory graded equipment. Kilic *et al.* [16] has presented a refractometer of an etched chirped Fiber Bragg Grating (FBG) in MCF, and exhibited a RI sensitivity of 1.43 nm/RIU with a detection limit of 2.4 $\times$ 10^{-6} RIU in the background RI of 1.316, moreover, temperature sensitivity can be compensated by the central core of MCF. In recent, we have reported two different kinds of interferometers related to eMCF; a RI sensor with temperature in-line compensation has displayed a RI sensitivity of 42.83 nm/RIU and temperature sensitivity of 9.89 pm/°C [19], and the other structure has displayed superior temperature sensitivity of 103.2 pm/°C in the range of 24 to 70 °C with an insensitive feature of RI in the range of 1.34 to 1.38 [20].

In this research, we propose a MZI structure based on an eMCF. The structure consists of a cascaded formation of single-multi-eMCF-multi-single mode fibers (SMEMS). In order to expose the outer cores of MCF, a slow etching technique [20], [21] is employed to fabricate the sensor. The eMCF is employed to generate coupled super-modes for stronger interference and enhanced the interaction of outer-core modes with surrounding medium. However, the proposed sensor can easily discriminate temperature and RI through inter-cross-demodulation, and also can function via multiplex configurations. The proposed work is the series of existing paper related to eMCF [20], upon experimental demonstrations the sensor poses repeatability and reproducibility. Whereas the MCF outer cores are exposed near to surrounding, the intensity response of RI is enhanced but temperature shift response decreases. By employing intensity and wavelength demodulations of inter-cross phenomena; the sensor can effectively sort the issues of cross-sensitivity.

The fabrication, working principle and simulation of the proposed SMEMS sensor are discussed in Section II. Experiment results are reported in Section III.

II. Principle of Operation

A. Sensor Fabrication

The schematic diagram of the SMEMS sensor and experimental setup is shown in Fig. 1. The proposed structure can be fabricated with subsequent steps. Step-1: Prior to the fusion of the fibers, a piece of MCF is independently etched using an etching technique reported in [20], [21]. Step-2: A SMF and an ordinary commercial step-index multimode fiber (MMF) are fused together, and the MMF is then cleaved at a distance of 2 mm. Step-3: By repeating the above procedure, two analogous sets of SMF-MMF segments are prepared. Then, these segments are deployed to be Lead-in (L/I) and Lead-out (L/O), respectively. Step-4: A pre-fabricated segment of eMCF of length 20 mm (diameter$\sim$76.4 μm) is then spliced in between SMF-MMF L/I and SMF-MMF L/O, so that SMEMS structure can be constituted, as shown in Fig. 1(a). Since handling of eMCF is difficult task due to fragility, but it is carefully cleaved by adjusting the blade position of an ordinary cleaver. Nowadays, different packaging platforms are available to handle the issue of fragility. The proposed eMCF is fragile somehow but have considerable strength compared with tapered fiber structures. All fusion splicing is performed with a commercial splicer device (COMCORE), a KEYENCE Digital microscope (VHX-100 series) is used to record the images of fibers, and the parameters of utilized fibers are listed in the Table. I. The cross-sectional images of MCF, eMCF and SMEMS sensor under the microscope can be seen in Fig. 2(a)–(c), respectively.

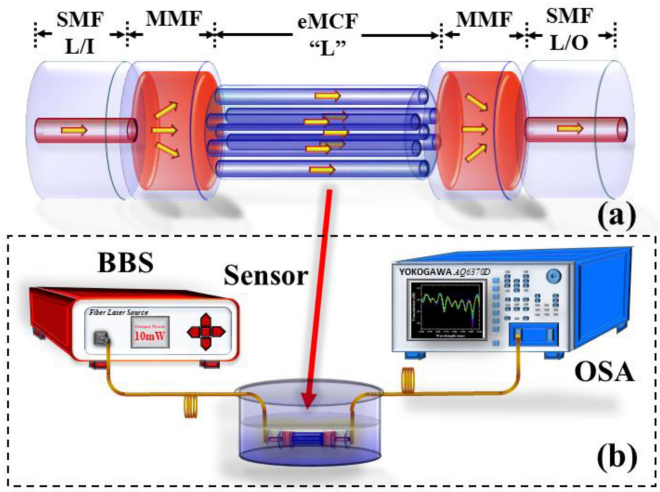

Fig. 1. (a) The schematic SMEMS senor and (b) experimental setup.

TABLE I
Fiber Parameters

Fibre Type	Diameter (µm)		Refractive index		Λ Pitch (µm)
	Core	Clad	Core	Clad	-
SMF	9	125	1.462	1.457	nil
MMF	105	125	1.444	1.439	nil
MCF	6.1	125	1.4681	1.4628	35
eMCF	6.1	76.4	1.4681	1.4628	35

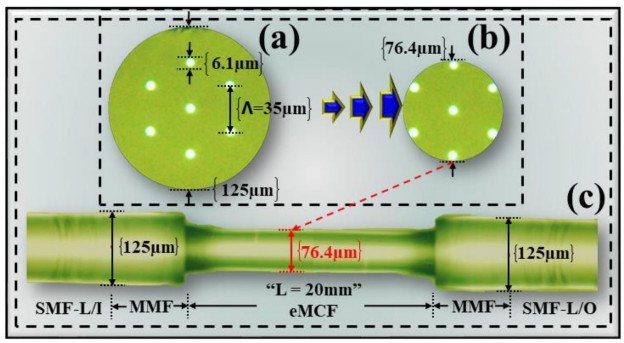

Fig. 2. Images under the microscope (a) MCF before etching, (b) eMCF after etching, and (c) SMEMS sensor.

B. Working Principle

When the light is launched from the SMF-MMF L/I toward eMCF, several modes can be excited due to a large core mismatch of SMF and MMF. MMF is an optical fiber that support multiple transverse guided mode for an applied frequency and its

guided modes can be determined by wavelength and refractive index profile. Here, for suitability, 2 mm of MMF's length is used to tailor the best spectral interference. Further, the excited multiple higher-order modes from MMF are degenerated in intensity while propagating through eMCF. Due to large core of MMF, it is expected that light intensity will be weakly coupled from the center to outer hexagonal distributed cores of eMCF. Here, we can realize that only two super-modes would mainly contribute to the interference, as the other higher-order modes will be degenerated due to circular symmetry of the eMCF cores and phase differences across the cores. The modal interference between two super-modes is continuously varied the spatial pattern, and finally when the light reaches at next MMF, the light re-couple back toward SMF L/O. Whereas the total light intensity received by an optical spectrum analyzer (OSA: YOKOGAWA AQ6370D) at the output, can be expressed as,

$$I_{total} = I_{ct} + I_{ot} + 2\sqrt{I_{ct} I_{ot}} \cos\theta \tag{1}$$

where I_{ct} and I_{ot} are the light intensities of the super-modes corresponding to center and outer core of the SMEMS sensor, respectively. The relative phase difference θ between the super-modes can be expressed as,

$$\theta = \frac{2\pi \Delta n_{eff}^{ct,ot} L}{\lambda} \tag{2}$$

where λ is the operating wavelength of the transmitted light from a broadband source (BBS), L is the length of the eMCF, and $\Delta n_{eff}^{ct,nt}$ represents the relative effective refractive index difference. $\Delta n_{eff}^{ct,nt}$ can be written as,

$$\Delta n_{eff}^{ct,ot} = n_{eff}^{ct} - n_{eff}^{ot} \tag{3}$$

where n_{eff}^{ct} is the effective refractive index of the center core super-mode and n_{eff}^{ot} is the effective refractive index of the relevant outer core super-mode. From Eq. (1), we have found that when the interference reaches to minimum intensity, then the phase difference between two super- modes should be equal to (2m+1) π while propagating through the eMCF of length L. Thus, the wavelength of the m^{-th} order attenuation peak can be written as,

$$\lambda_m = \frac{2\Delta n_{eff}^{ct,ot} L}{2m+1} \tag{4}$$

Here, λ_m is the resonant wavelength, which is directly related to the eMCF of length L. From Eq. (4), the free spectral range (FSR) of the proposed MZI sensor can be estimated as,

$$FSR = |\lambda_m - \lambda_{m-1}| \approx \frac{{\lambda_m}^2}{\Delta n_{eff}^{ct,ot} L} \tag{5}$$

C. Simulation and Interference Spectrum

The working principle is simulated by a Beam propagation module (BPM). The simulated results are explained that when the light enters from SMF-MMF L/I toward eMCF, the multimode interference is generated at first MMF. Then, the light will not be only remained in the center core but also spread into the outer cores, and the cladding of eMCF. As a result, when

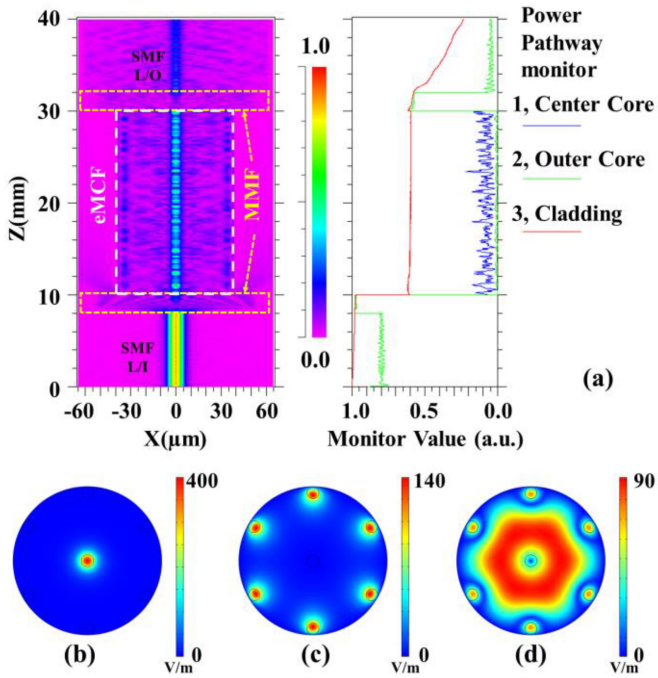

Fig. 3. Simulated profile of SEMES sensor (a) Beam propagation describes the power distribution of the center core, outer core and cladding region while propagating through sensor; and the transverse E-field of the eMCF for (b) center core mode, (c) outer cores super-mode, and (d) the partially coupled outer core and cladding supper-mode.

such two distinct beams will interfere each other to form an MZI interferometer, as shown in Fig. 3(a). It can be realized that when the multi-mode interference would excite from MMF toward eMCF. Most of the higher-order modes are found to be degenerate in intensity while propagating through eMCF. Whereas the theoretical agreement has also explained; due to different phases across the cores, mostly higher-order modes will be degenerated. Nevertheless, such modal interference can play a vital role to attain a strong interference pattern. Also, it can be seen that when the light propagates through eMCF toward SMF L/O via MMF, only two dominant super-modes could propagate in the sensing probe, which are center and outer core modes, as traced by the power pathway monitor in Fig. 3(a). In order to obtain a direct interaction between outer cores and surrounding medium, the eMCF is deployed. As a result, the evanescent field will become stronger at the eMCF clad-surrounding interface. Moreover, the simulated transverse electric (E) field distribution of fundamental super-modes are obtained, as shown in Fig. 3(b)–(c). Also, the light intensity has to be partially coupled among outer cores and cladding of the eMCF. For realization, we have also obtained the transverse E-field distribution of the couple cladding mode, as shown in Fig. 3(d). Therefore, we can realize from the simulations that the power distribution in the proposed SMEMS sensor has clarified the coupling and recoupling phenomena of light intensity at SMF-MMF-L/I and SMF-MMF-L/O, respectively. Also, such spatial variation of modal interference will substantially take part to form a stronger MZI interference pattern. The interference transmission spectra of the SMEMS sensor under different

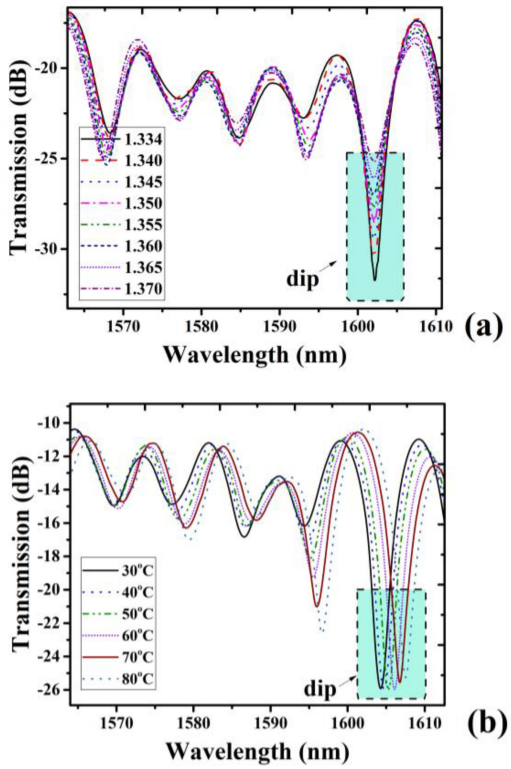

Fig. 4. Transmission interference spectra of the SMEMS sensor (a) under different surrounding RI and (b) under air with temperature rise.

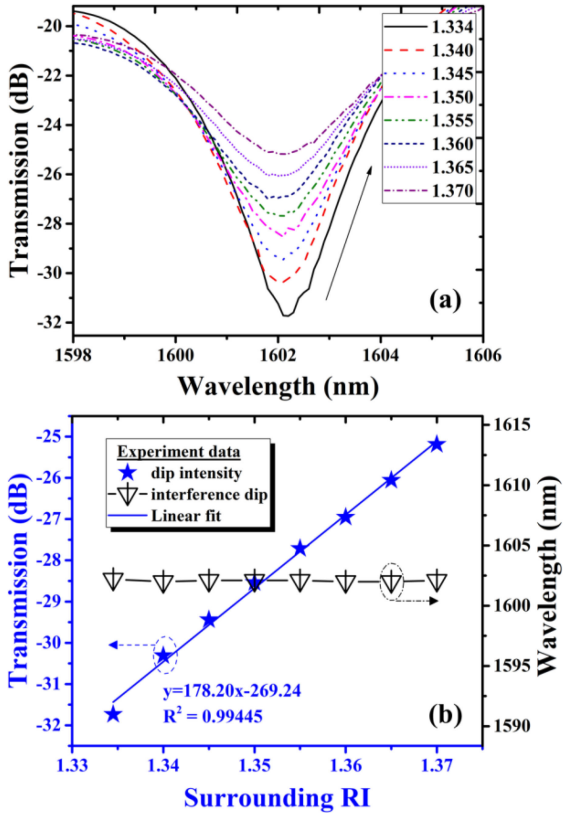

Fig. 5. (a) Transmission spectrum evolution of the SMEMS sensor under different surrounding RI; (b) measured sensitivity with dip intensity change and linear fit at room temperature.

surrounding RI and under air with temperature rise are recorded by an OSA, as shown in Fig. 4(a)–(b) respectively.

III. Experiment and Discussion

The experimental setup of the proposed SMEMS sensor for RI measurement is shown in Fig. 1(b). A BBS with a laser wavelength range from 1540 to 1610 nm, and an OSA are employed to monitor the transmission spectrum of SMEMS sensor. In order to investigate the surrounding RI, we have calibrated a series of RI solution in the range of 1.334 to 1.370 using an Abbe refractometer. A percentage of glycerol is added into deionized water to calibrate different RI solution by Zinah's method [8]. The interference dip variation with respect to different surrounding RI is plotted in Fig. 4. It can be observed that resonant interference dip has slightly fluctuated in wavelength at different surrounding RI, but a large variation occurred in wavelength intensity. Whereas the RI fluctuations in wavelength might be affected due to external temperature error ± 0.00255 °C. Also, the intensity shift of resonant interference dip at different surrounding RI has displayed a good agreement of a linear fit response. The inset of resonant dip with RI changes is taken from Fig. 4, which can be seen in Fig. 5(a). Whereas the RI sensitivity of SMEMS sensor has exhibited as 178.20 dB/RIU in the range of 1.334 to 1.370, with a linear fitting of 0.9945, as shown in Fig. 5(b). Compared with several previously reported RI sensors (27 dB/RIU [10], 94.58 dB/RIU [11], -74.2 dB/RIU [12], and -110 dB/RIU [22]), the proposed sensor is substantially enhanced and improved the sensitivity.

Afterward, in order to investigate the temperature response of SMEMS sensor; the sensor is placed into a heating furnace, whose temperature error is ± 0.01 °C. We have measured the temperature in the range of 30 to 80 °C with an increment of 5 °C during each heating. Whereas the temperature is kept for 10 min during each increment of heating. When the temperature rose, the resonant dip has linearly shifted toward a longer wavelength, but the dip intensity has hardly changed. During experimental demonstration, we have observed that the temperature has induced a "redshift" in the wavelength. However, the redshift is found obvious due to the material characteristic of MCF. As the thermo-optic coefficient of the Ge-doped silica core is higher than the fused silica cladding, so the effective refractive index difference between the core and cladding modes has become large with surrounding temperature change [23]. Since the thermo-optic coefficient of the center core of a MCF is higher, so it could have formed a large difference of effective refractive index between center core and surrounding medium. Correspondingly it could effectively enhance the temperature sensitivity. The theoretical relationship between the temperature and resonant interference dip can be calculated as [20],

$$\frac{d\lambda}{d\mathrm{T}} = \frac{\lambda}{\Delta n_{eff}^{ct,ot}} \left[\frac{dn_{eff}^{ct}}{d\mathrm{T}} - \frac{dn_{eff}^{ot}}{d\mathrm{T}} \right] \tag{6}$$

From Fig. 6(a), It can be inferred that the resonant interference dip of SMEMS sensor has linearly shifted toward the longer

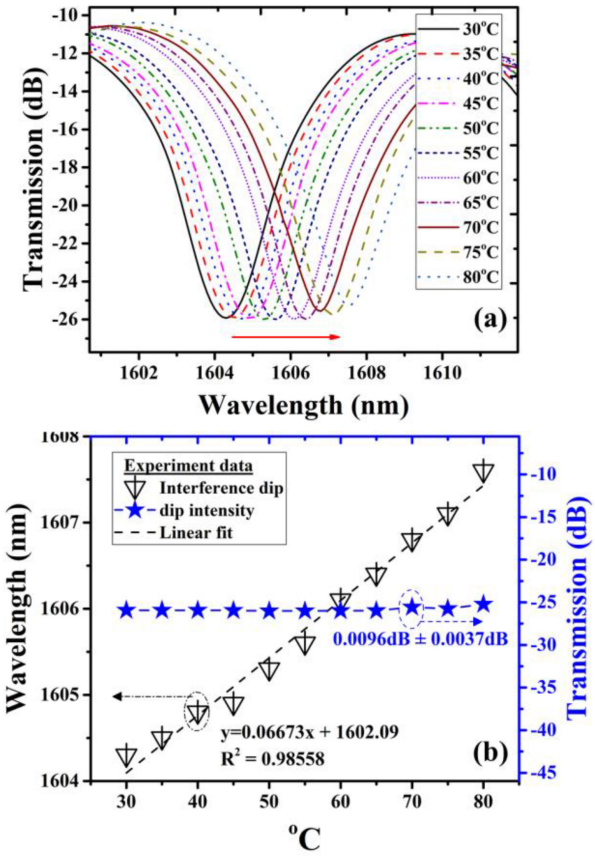

Fig. 6. (a) Transmission spectrum evolution of the SMEMS sensor under surrounding temperature change; (b) measured sensitivity with dip wavelength shift and dip intensity, and their linear fit responses.

wavelength with temperature rose, but the dip intensity could have rarely changed within ±0.0037 dB, which is negligible. Besides, the sensor has displayed temperature sensitivity 66.73 pm/°C in the range of 30 to 80 °C with a linear fitting of 0.9856, as shown in Fig. 6(b).

After the experimental demonstrations, we have found that the proposed SMEMS sensor can be a potential candidate for a multiplex configuration of the inter-cross-demodulation system and support operations under three different demodulation phenomena, which are as follows:

1) Simultaneous measurement of RI and temperature by intensity and wavelength demodulation, respectively.
2) Temperature in-sensitive and RI sensitive by intensity demodulation.
3) RI in-sensitive and temperature sensitive by wavelength demodulation.

Besides, we haven't found any serious deterioration in transmission spectra and the extinction ratio, with variation of surrounding RI and temperature rose. Also, the sensor has been solved the issue of cross-sensitively.

IV. Conclusion

In summary, the proposed SMEMS sensor based on an eMCF structure of a MZI principle has been realized to achieve the RI and temperature measurement. The slow etching technique is employed to fabricate the sensor. The sensor exhibits RI sensitivity ∼178.20 dB/RIU in the range of 1.334 to 1.370 and temperature sensitivity ∼66.73 pm/°C from 30 to 80 °C. Besides, SMEMS sensor has displayed the merits of easy fabrication, stable response, and nil cross-sensitivity. The stability and nil cross-sensitivity features indicate that the proposed sensor is a promising candidate, and may find potential applications in various fields of science, such as ocean engineering, chemical inspection, biomedicine and etc.

Disclosures

No potential conflict of interest was reported by the authors.

References

[1] M. del Carmen Alonso-Murias, J. S. Velázquez-González, and D. Monzón-Hernández, "SPR fiber tip sensor for the simultaneous measurement of refractive index, temperature, and level of a liquid," *J. Lightw. Technol.*, vol. 37, no. 18, pp. 4808–4814, Jun. 2019.
[2] Y. Zhang *et al.*, "Simultaneous measurement of temperature and refractive index based on a hybrid surface plasmon resonance multimode interference fiber sensor," *Appl. Opt.*, vol. 59, no. 4, pp. 1225–1229, Feb. 2020.
[3] Y. Cao, H. Zhang, Y. Miao, Z. Ma, and B. Li, "Simultaneous measurement of temperature and refractive index based on microfiber Bragg Grating in Sagnac loop," *Opt. Fiber Technol.*, vol. 47, pp. 147–151, Jan. 2019.
[4] B. Shang, Y. Miao, H. Zhang, and L. Zu, "Structural modulated ultralong period microfiber grating for the simultaneous measurement of the refractive index and temperature in a low-refractive-index range," *IEEE Sensors J.*, vol. 20, no. 3, pp. 1329–1335, Feb. 2020.
[5] R. Zhang, S. Pu, and X. Li, "Gold-film-thickness dependent SPR refractive index and temperature sensing with hetero-core optical fiber structure," *Sensors*, vol. 19, no. 19, Jan. 2019, Art. no. 4345.
[6] D. Guo *et al.*, "Tapered multicore fiber interferometer for refractive index sensing with graphene enhancement," *Appl. Opt.*, vol. 59, no. 13, pp. 3927–32, May 2020.
[7] P. Cheng *et al.*, "Refractive index interferometer based on SMF-MMF-TMCF-SMF structure with low temperature sensitivity" *Opt. Fiber Technol.*, vol. 57, Jul. 2020, Art. no. 102233.
[8] Z. A. Al-Mashhadani and I. Navruz, "Highly sensitive measurement of surrounding refractive index using tapered trench–assisted multicore fiber," *Opt. Fiber Technol.*, vol. 48, pp. 76–83, Mar. 2019.
[9] J. Kang, J. Yang, X. Zhang, C. Liu, and L. Wang, "Intensity demodulated refractive index sensor based on front-tapered single-mode-multimode-single-mode fiber structure," *Sensors*, vol. 18, no. 7, Jul. 2018, Art. no. 2396.
[10] Z. L. Ran, Y. J. Rao, W. J. Liu, X. Liao, and K S. Chiang, "Laser-micromachined Fabry–Perot optical fiber tip sensor for high-resolution temperature-independent measurement of refractive index," *Opt. Express*, vol. 16, no. 3, pp. 2252–2263, Feb. 2008.
[11] H. Xue, H. Meng, W. Wang, R. Xiong, Q. Yao, and B. Huang, "Single-mode-multimode fiber structure based sensor for simultaneous measurement of refractive index and temperature," *IEEE Sensors J.*, vol. 13, no. 11, pp. 4220–4223, May 2013.
[12] J. Madrigal, D. Barrera, and S. Sales, "Refractive index and temperature sensing using inter-core crosstalk in multicore fibers," *J. Lightw. Technol.*, vol. 37, no. 18, pp. 4703–9, May 2019.
[13] S. Pevec and D. Donlagic, "High resolution, all-fiber, micro-machined sensor for simultaneous measurement of refractive index and temperature," *Opt. Express* vol. 22, no. 13, pp. 16241–16253, 2014.
[14] J. S. Velázquez-González, D. Monzón-Hernández, D. Moreno-Hernández, F. Martínez-Piñón, and I. Hernández-Romano "Simultaneous measurement of refractive index and temperature using a SPR-based fiber optic sensor. *Sensors Actuators B: Chem.*, vol. 242, pp. 912–920, Apr. 2017.
[15] D. A. May-Arrioja and J. R. Guzman-Sepulveda" Highly sensitive fiber optic refractive index sensor using multicore coupled structures," *J. Lightw. Technol.*, vol. 35, no. 13, pp. 2695–701, Jul. 2017.
[16] S. G. Kilic, Y. Zhu, Q. Sheng, M. N. Inci, and M. Han, "Refractometer with etched chirped fiber bragg grating Fabry–Perot interferometer in multicore fiber," *IEEE Photon. Technol. Lett.*, vol. 31, no. 8, pp. 575–8, Feb. 2019.

[17] C. Zhang *et al.*, "Etching twin core fiber for the temperature-independent refractive index sensing," *J. Opt.*, vol. 20, no. 4, Mar. 2018, Art. no. 045802.
[18] B. Dai *et al.*, "Temperature-insensitive refractive index sensor with etched microstructure fiber," *Sensors*, vol. 19, no. 17, Jan. 2019, Art. no. 3749.
[19] W. Hu, C. Li, S. Cheng, F. Mumtaz, C. Du, and M. Yang, "Etched multicore fiber Bragg gratings for refractive index sensing with temperature in-line compensation," *OSA Continuum*, vol. 3, no. 4, pp. 1058–1067, Apr. 2020.
[20] F. Mumtaz *et al.*, "A design of taper-like etched multicore fiber refractive index-insensitive a temperature highly sensitive Mach–Zehnder interferometer," *IEEE Sensors J.*, vol. 20, no. 13, pp. 7074–7081, Jul. 2020.
[21] E. J. Zhang, W. D. Sacher, and J. K. Poon, "Hydrofluoric acid flow etching of low-loss subwavelength-diameter biconical fiber tapers," *Opt. Express*, vol. 18, no. 21, pp. 22593–22598, Oct. 2010.
[22] S. Silva, O. Frazão, J. L. Santos, and F. X. Malcata, "A reflective optical fiber refractometer based on multimode interference," *Sensors Actuators B: Chem.*, vol. 161, no. 1, pp. 88–92, Jan. 2012.
[23] P. Lu, L. Men, K. Sooley, and Q. Chen., "Tapered fiber Mach–Zehnder interferometer for simultaneous measurement of refractive index and temperature," *Appl. Phys. Lett.*, vol. 94, no. 13, Mar. 2009, Art. no. 131110.

Farhan Mumtaz was born in Islamabad, Pakistan, in 1985. He received the B.Sc. degree from the University of Punjab, Lahore, Pakistan and the M.Phil. degree in electronics from Quaid-i-Azam University, Islamabad, Pakistan, in 2006 and 2018, respectively. Currently he is working toward the Ph.D. degree program in information and communication engineering with the Wuhan University of Technology, China. Besides that, he has more than nine years of professional experience at Huawei Technologies, Pakistan serving on positions like Senior Manager Service Solution Sales, Project Manager, and Planning Control Manager. His current area of research interests include the design of optical fiber based sensors, optical waveguide, EMT-Scattering, theoretical and computational electromagnetics, and electromagnetic compatibility.

Yutang Dai was born in Hubei Province, China, in 1965. He received the master's degree from the Huazhong University of Science and Technology, China, and the Ph.D. degree from the Nippon Institute of Technology, Japan, in 1989 and 2001, respectively. Then, he researched the ultra-precision micromachining technique of optoelectronic materials for four years at the Institute of Physical and Chemical Research (RIKEN), Japan. Presently, he is serving as an Professor with the National Engineering Laboratory of Fiber Optical Sensing technology, Wuhan University of Technology, China. His current interests include femtosecond laser micromachining of optoelectronic materials and the development of new-type fiber optical sensors.

Muhammad Aqueel Ashraf received the Ph.D. degree in electronics from Quaid-i-Azam University, Islamabad, Pakistan. He is currently serving as an Associate Professor with the Department of Electronics, Quaid-i-Azam University, Islamabad, Pakistan. He has extensively worked in the domain of electromagnetics, communication and optics. His area of research specialty includes waveguide optics, communication, antenna, and wave propagation, electromagnetic scattering, and computational EMT.